https://doi.org/10.1016/j.apenergy.2019.114197

Title: Coal pretreatment and Ag-infiltrated anode for high-performance hybrid direct coal fuel cell

Heping Xie [1,2*], Shuo Zhai [1], Bin Chen [2], Tao Liu [1], Yuan Zhang [4], Meng Ni [3], Zongping Shao [4]

[1]Institute of New Energy and Low-Carbon Technology, Sichuan University, Chengdu 610065, China.

[2]Guangdong Provincial Key Laboratory of Deep Earth Sciences and Geothermal Energy Exploitation and Utilization, Institute of Deep Earth Sciences and Green Energy, Shenzhen University, Shenzhen 518060, China.

[3]Building Energy Research Group, Department of Building and Real Estate, The Hong Kong Polytechnic University, Hung Hom, Kowloon, Hong Kong, China.

[4]State Key Laboratory of Materials-Oriented Chemical Engineering, College of Chemical Engineering, Nanjing Tech University, Nanjing 210009, China.

[*]Corresponding authors: xiehp@szu.edu.cn (H.X.)

Abstract:

Hybrid direct coal fuel cells (HDCFCs) have the potential to convert coal into electrical power in a clean and efficient manner. However, the related coal pretreatment method and the anode activity should both be improved, before the HDCFCs could match the performance of other direct coal fuel cells such as those based on solid oxide. In this study, we pyrolysed bituminous coal at 800°C followed by modification with acetic acid, in order to remove organic volatiles and reintroduce surface functional groups, respectively. The result was a modified char that was highly pure and with high oxidation activity. Further, the $(Y_2O_3)_{0.08}(ZrO_2)_{0.92}$ anode was infiltrated with Ag nanoparticles as an effective catalyst to promote the electro-oxidation of carbon. Under optimised conditions, the HDCFC with Ag-infiltrated anode and modified char as fuel demonstrated a maximum power density (403 mW cm^{-2} at 750°C) that exceeds previous results for coal-based fuels. The cell also showed stable operation for 14 hours, with a fuel conversion of 97.22% and Faradic efficiency of 61.06% using 0.4 g modified char.

Keywords:

Direct carbon fuel cell, coal pretreatment, nanosized Ag infiltration, high fuel conversion, Faradic efficiency

1. Introduction

The environmental contamination and energy dilemma have created a need for clean and highly efficient utilisation of traditional fossil fuels, such as petroleum and coal, which remain significant energy sources today. Coal, a major natural form of carbon, has massive reserves and the unique advantages of high volumetric energy density and convenience in storage and transportation [1]. Direct carbon fuel cell (DCFC) is a promising electrochemical equipment that converts chemical energy in solid carbon to electric energy without combustion [2]. Compared with traditional coal-fired power station, the direct carbon fuel cell has low emission, low noise, and high efficiency [3]. While the theoretical energy efficiency is 100%, a value up to 80% has been achieved in practical operation [4].

The overall reaction in a DCFC is shown in Eq. (1):

$$C + O_2 = CO_2 \tag{1}$$

The DCFCs can be classified according to the electrolyte, such as solid oxide (SOFC), molten carbonate (MCFC), molten hydroxide (MHFC), and hybrid direct carbon fuel cell (HDCFC) [5]. Among these, the HDCFCs are gaining increasing attention due to their high-power density and high carbon utilisation rate, because they extend the electrochemically reactive sites from the solid carbon-anode interface (e.g. SOFC) to the huge molten carbonate-carbon interface [6]. With the addition of molten carbonate to the carbon, the anodic reaction mechanism in a HDCFC becomes quite complex and concepted as “hybrid”, of which the actual mechanism can be the combination of (**i**) carbon electrochemical oxidation by oxygen ions at the contact of carbon and solid electrolyte (Eq. (2) and Eq. (3)); (**ii**) oxidation by carbonate ions from the molten carbonates via Eq. (4) and Eq. (5); (**iii**) the enhanced CO electrochemical reactions(Eq.(7) and Eq.(8)) driven by the reversed Boudouard reaction (Eq. (6)) for which the CO_2 can be provided by the carbonate decomposition [7].

$$C + 2O^{2-} = CO_2 + 4e^- \tag{2}$$

$$C + O^{2-} = CO + 2e^- \tag{3}$$

$$C + 2CO_3^{2-} = 3CO_2 + 4e^- \quad (4)$$

$$C + 2CO_3^{2-} = CO + CO_2 + 2e^- \quad (5)$$

$$C + CO_2 = 2CO \quad (6)$$

$$CO + O^{2-} = CO_2 + 2e^- \quad (7)$$

$$CO + CO_3^{2-} = 2CO_2 + 2e^- \quad (8)$$

The neutral charge of molten carbonate in case of Eq. (4) and Eq. (5) is maintained by the regeneration of CO_3^{2-} ion [8], as shown in Eq. (9):

$$CO_2 + O^{2-} = CO_3^{2-} \quad (9)$$

The required oxygen ions are migrated from the cathode where oxygen is reduced:

$$O_2 + 4e^- = 2O^{2-} \quad (10)$$

Compared to the gas-fuelled SOFCs, the DCFC has encountered more challenges, such as a large mass transfer resistance and a poor solid fuel electro-oxidation activity [9]. Currently, most studies have focused on utilising pure carbon, such as activated carbon [10], graphite [11], and carbon black [12] as the fuel. Nevertheless, the goal of the DCFC technology is to directly use coal [13]. In coals, impurities such as iron oxide, magnesium oxide, and calcium oxide have been demonstrated as favourable catalysts for the reversed Boudouard reaction [14]. However, ashes in coal such as Al_2O_3 and SiO_2 can accumulate in the anode after the carbon is consumed, leading to blocked mass transport, corrosion, and consequently a decline of cell performance [6]. Besides, the sulfur contained in raw coal could poison the anode catalyst (such as the vulnerable Ni). Therefore, it is necessary to pretreat the coal to remove the unwanted impurities. Pyrolysis is a common coal pretreatment method. During the pyrolysis, most organic volatile products are removed as tars or other gaseous and condensable species, while the inorganic mineral composition mainly remains in the coal char [15]. Nevertheless, the structure and surface properties of carbon change greatly during this process, including the increase of graphitisation and the loss of surface functional groups, which will decrease the oxidation activity of coal [16]. Acid treatment is considered as a good complement to pyrolysis that can both remove the impurities and improve the oxidation activity. Dudek used nitric acid to remove impurities from the coal sample, reducing the ash

content from 3 wt.% to 0.4 wt.% to achieve better performance [17]. Fan et al. also pre-treated coal with HNO_3 and found that the improved power density might be due to the increased content of oxygenated functional groups [18]. These findings show that acid treatment can improve the electrochemical performance of coal-based fuel cells by removing ash and activating the carbon particles. However, Common inorganic acids such as Nitric acid are not environmentally friendly substance and the performance of previously reported DCFCs using coal as fuel was still much lower than that of SOFCs using gaseous fuel in terms of power density and durability. Therefore, the anode electrode and coal pretreatment should be further optimised to address these issues in DCFCs.

Herein, we report a high-performance bituminous coal-fuelled HDCFC using the triple strategies of coal pyrolysis, acetic acid coal pretreatment, and anode silver nanoparticle infiltration. The combined pyrolysis and acetic acid pretreatment were found to improve the applicability of coal-derived solid fuel in HDCFCs, while the Ag boosted the *in-situ* coal gasification by using traditional Ni/YSZ anode-supported single cell. Bituminous coal, pyrolyzed char, and modified char were used as fuel at 750 °C. The cell with modified char showed the excellent performance with a maximum power density of 366 mW cm^{-2}. To further improve the anode performance, a modified cell that had infiltrated silver nanoparticles on the Ni-YSZ anode was tested. The as-developed HDCFC demonstrated a maximum power density of 403 mW cm^{-2} using modified char at 750 °C. Under the optimised conditions, the HDCFC can be operated continuously for more than 14 h.

2. Experimental

2.1. Fuel preparation

Three kinds of carbons have been used, raw bituminous coal, coal char, and modified coal char. Raw bituminous coal was collected from one coal seam at a depth of 1050 meters from the Pingding Mountain mining area (Shanxi Province, China). The coal was milled and passed through 150-mesh standard sieve before use.

The coal char was produced from the pyrolysis of raw bituminous coal. The raw coal was put in a horizontal tubular furnace and heated to 800℃ in an argon atmosphere (30 mL min^{-1}) at a heating rate of 10℃ min^{-1}, then kept at 800℃ for 4 h. After cooling to room temperature, the coal char was

ground by a ball mill and further sieved with a 150-mesh steel sieve.

The modified coal char was derived from the coal char by acid modification. Fine coal char was initially soaked in 2 mol L^{-1} acetic acid solution with a mass ratio of 0.2 at 40℃ for 20 h. Then, the mixture was washed with deionised water. After a neutral pH was achieved, the modified coal char was dried at 80℃ about 12 h and passed through a 150-mesh sieve.

Each coal-based fuel was mixed with a eutectic mixture of 62 mol% lithium carbonate (Aladdin Reagents, analytical grade) and 38 mol% potassium carbonate (Aladdin Reagents, analytical grade) at a carbon-to-carbonate weight ratio of 1:0.25 by ball milling in isopropanol for 1 h. The final carbon-carbonate mixture was dried at 80℃ about 12 h.

2.2. Fuel characterisation

The metal content in the different fuels was examined via inductively coupled plasma optical emission spectrometer (ICP-OES). Organic elemental analysis was carried out using a Vario EL cube. The phase compositions and crystallinity of the fuels was examined by X-ray diffraction (XRD, Bruker AXS D8 Advance A25X) analysis with Cu Kα radiation (λ = 0.15418 nm). The surface property of the fuels was examined via a Fourier transform infrared (FTIR) spectrometer (Perkin-Elmer) in the region of 4000–400 cm^{-1}. Raman experiments were performed with a Renishaw inVia reflex with an excitation wavelength of 532 nm. Nitrogen adsorption experiments were carried out using a Micromeritics ASAP 2460 instrument with N_2 physical adsorption at 77 K. Scanning electron microscope (SEM) images of the different fuels were characterised by FEI Inspect F50. Thermogravimetric analysis (TGA) was conducted in a TGA5500 thermobalance. The weight loss data was collected under CO_2 (20 mL min^{-1}) as carrier gas and heated to 800℃ at a rate of 20℃ min^{-1} and held for 30 min.

2.3. Powder synthesis

Both $SrSc_{0.175}Nb_{0.025}Co_{0.8}O_{3-d}$(SSNC) and $Sm_{0.2}Ce_{0.8}O_{1.9}$(SDC) perovskite powders were synthesised via a sol-gel method and the detailed synthesis process has been described elsewhere [19]. Pure SSNC and SDC phase was obtained by calcination of their black precursor at 900℃ and 700℃ for 5 h in air respectively.

2.4. Fuel cell fabrication

A tape-casting process was used to prepare single fuel cells with anode support. The anode slurry was prepared with commercial NiO (Aladdin Reagents, analytical grade), $(Y_2O_3)_{0.08}(ZrO_2)_{0.92}$ (YSZ, Tosoh), starch, and triethanolamine in a mass ratio of 60:40:10:3. The mixed powder was first ball-milled with ethanol and dimethylbenzene for 24 h. Then, polyvinyl butyral, polyethylene glycol, and dibutyl ophthalate in a mass ratio of 14:10:13 were added to the resultant slurry. After being milled again for 24 h, the mixture was poured over a tape and placed in air for 12h. "Then the substrates were punched into disks with a diameter of 16 mm, followed by calcining at 1000°C for 2 h with the thickness shrunk to 0.4 mm. A thin-film YSZ electrolyte layer (~8 μm) was deposited onto each substrate and then sintered at 1400°C for 5 h in air. Next, the SDC interlayer (~4 μm) was deposited onto the YSZ electrolyte side. The NiO-YSZ/YSZ/SDC half-cell was sintered at 1350°C for 2 h in air. Finally, the SSNC cathode slurry was screen-printed onto the centre of the SDC layer (with a circular area of 0.5 cm^2 and a thickness of ~10 μm), followed by sintering at 900°C for 2 h in air atmosphere." The detailed synthetic procedure of the single cells has been described elsewhere [20].

2.5. Preparation of anode catalyst solution and infiltration

A 0.5 mol L^{-1} solution of $AgNO_3$ in deionised water was prepared for infiltration. An appropriate amount of glycine was added to the solution to facilitate the formation of the desired oxide phase at relatively low temperatures. The $AgNO_3$ solution was infiltrated into the pores of the porous anode structure under vacuum, using a microliter syringe to control the loading amount. The infiltrated cells were sintered at 400°C for 30 min. The above process was repeated four times, and finally the cells were sintered at 900°C for 2 h to obtain the desired nanocrystalline phase of AgO. After reduction in hydrogen atmosphere (the detailed reduction process of the single cells shows in the next section), well-distributed Ag nanoparticles were formed. Overall, the Ag nanoparticles-infiltrated anode was fabricated through a tape-casting and infiltration method, as visually summarised in Fig. 1(a).

2.6. HDCFC assembly and testing

Silver wires were connected to both sides of the cell, after painting silver paste on the cathode to act as a current collector. Each cell was sealed on one end of a quartz tube with silver paste as jointing and sealing material, as shown in Fig. 1(b). Then the fuel cells went through a prereduction stage:

the furnace was heated from room temperature to target temperature at rate of 5°C min^{-1} under H_2 atmosphere for 30 min, after that they were cooled to room temperature at the same condition. Carbon-carbonate mixture (0.5 g) was filled into the anode side of the HDCFC. The fuel cells were tested with the following procedure. An N_2 flow of 5 mL min^{-1} was used as the anode atmosphere, whereas ambient air was used in the cathode side. The furnace was heated from room temperature to 750°C at a 10°C min^{-1} rate, and then maintained at 750°C. The electrochemical performance data, including the I-V curves, electrochemical impedance spectra (EIS), and discharge curve were collected by a four-probe method using via a Solartron 1287 Electrochemical Workstation. The voltage amplitude was 10 mV and the applied frequency range of electrochemical impedance spectra was from 0.1 Hz to 100 kHz. The microstructures of the Ag-infiltrated cells after reducing in H_2 atmosphere were characterised by SEM (FEI Inspect F50, USA). FIB was used as site specific sample preparation method for further examined by transmission electron microscopy (TEM) measurements. Two instruments were used: FEI HELIOS NanoLab 600i and FEI Titan G2 60-300.The phase structure of the modified char and carbonate mixture before and after electrochemical constant current discharge test was examined by XRD.

3. Results and discussions

3.1 Properties of different carbon samples

3.1.1 Elemental analysis

The contents of organic elements and major metals are shown in Table 1 and Fig. 2, respectively. In Table 1, the carbon content in modified char (89.18 wt.%) is much higher than that of bituminous coal (80.99 wt.%) and char (84.71 wt.%). It is important to note a higher carbon content also means that the same quantity of coal can produce more electricity. The acetic acid treatment increased the atomic content of H by 1.2 wt.% and decreased that of oxygen by 1.26 wt.%, and these results may be related to the change of hydroxyl functional groups and oxide content. In addition, in Fig. 2 the modified char showed much lower metal contents than the raw coal and char. For example, 83.83 wt.% of Si and 64.28 wt.% of Al were removed after the acetic acid treatment. These results prove that the acetic acid treatment method is effective for eliminating the ash contents in raw bituminous coal.

3.1.2 Carbon crystalline structure and mineral phases

XRD was used to examine the structure and mineral phase of the fuel samples. As shown in Fig. 3(a), in the bituminous coal three kinds of minerals were detected: calcite ($CaCO_3$), ankerite ($Ca_{0.997}(Mg_{0.273}Fe_{0.676}Mn_{0.054})(CO_3)_2$), and kaolinite ($Al_2Si_2O_5(OH)_4$). After the thermal treatment, the minerals were pyrolyzed to form oxides, and thus, only the peaks of calcium oxide (CaO) were observed for the char. For the modified char, no peaks of mineral matter were observed, because the metal oxides were dissolved by the acetic acid. In all three samples, there were two characteristic diffraction peaks of carbon crystalline structures at 2θ = 26° and 43°. The former peak is assigned to the (002) diffraction peak of graphite carbon, and the latter to the (100) diffraction peak of amorphous carbon [21]. The observed widening of these two peaks after pyrolysis and acid treatment suggests that the crystalline structures of carbon became more disordered, which could benefit carbon electrochemical oxidation in the HDCFC.

Raman spectroscopy analysis was further undertaken to unveil the crystalline structure of the samples. As shown in Fig. 3(b), the spectrum typically exhibits two characteristic peaks: the G (graphite) band and D (disordered) band situated respectively at around 1580 and 1350 cm^{-1}. The G band represents the vibrations of carbon atoms with sp^2-bonds in the plane of graphitic lattice, and the D band represents carbon atoms with dangling bonds at the edge of the disordered graphite lattice in the disordered graphite lattice [22]. It is well known that the peak intensity ratio $I_{(D)}/I_{(G)}$ is strongly associated with the degree of carbon graphitization, where a larger $I_{(D)}/I_{(G)}$ corresponding to a less graphitized structure. The $I_{(D)}/I_{(G)}$ values of the bituminous coal, char, and modified char samples are about 0.850, 0.921, and 0.946, respectively, indicating that the modified char has the largest amount of disordered carbon, which could enhance the carbon electrochemical oxidation activity. It is important to note that there was an increase in $I_{(D)}/I_{(G)}$ from coal to char, while a decrease is expected. Such behaviour was also observed by Livneh et al. [23]. Those authors speculated that the size and quantity of amorphous carbon crystallites in raw coal may be too small for effective coupling with the incident laser beam, and thus they contribute little to the Raman spectrum. After the carbon material was annealed to a certain temperature (about 800°C), the particle size of amorphous carbon increased to contribute to the Raman spectrum, which led to an increase in the ratio.

3.1.3 Chemical functional groups

The chemical structures of carbon fuels were studied using FTIR. As seen in Fig. 4, the spectrum of

bituminous coal reveals the following vibrational bands: 3436 cm^{-1} for O-H stretching vibration in hydroxyl functional groups, 2918 and 2854 cm^{-1} for CH_2 and CH_3 asymmetric and symmetric stretching vibrations in alkyl chains respectively, 1616 cm^{-1} for C=O (conjugated with C=C bonds) stretching vibrations, 1436 cm^{-1} for CH_2 and CH_3 deformation vibrations, and 1300–1000 cm^{-1} for various function groups containing C-O such as ethers, phenols, and hydroxyl groups [24,25]. After the transformation from coal to char, most of the functional groups in bituminous coal disappeared since the organic volatile products were largely eliminated. The modification with acetic acid led to an increase in the hydroxyl functional group (3436 cm^{-1}), which is consistent with the increase of H percentage from 1.61% to 2.78%. However, the O percentage decreased from 2.87% to 0.61%, which may because of the dissolution of metal oxides.

To better evaluate the fuel conversion process and understand its effects on the surface chemistry, the relative proportions of various functional groups should be calculated and compared among the fuel samples [26]. The band at about 1630 cm^{-1} representing the C=O stretching vibrations was taken as the reference and used to normalise the total peak area of the two oxygen-containing functional groups (O-H stretching and C-O stretching vibrations). As shown in Table 2, the calculated ratios of char and modified char are 14.22 and 20.76, respectively. It is well known that the carbon oxidation reaction is more likely to occur at carbon atoms connected with oxygen-containing functional groups, reside in alkyl chains, or exist at the edge/surface with dangling bonds. Therefore, the modified coal with its larger peak area ratio should have the most active sites for carbon electrochemical oxidation reaction among the three samples [21].

3.1.4 Textural structure and morphology

The surface textures of the three carbon samples, including specific surface areas, total pore volumes, and average pore sizes were determined by the adsorption of N_2 at 77 K, as seen in Table 3. The specific surface area was reduced after acid treatment, in good agreement with the results of Eom et al. [27], in which hydrochloric and nitric acid treatment of bituminous coal would reduce the specific surface area and porosity due to the collapse of pore walls on the fuel surface. In the SEM images for the three samples in Fig. 5, there is a clear variation in the particle size among the bituminous coal, char, and modified char, and the particle size of modified char is the smallest. No obvious pores were observed on the surfaces of the three samples, which is consistent with their low specific surface area in N_2 adsorption experiments.

3.1.5 Thermogravimetric analysis

To investigate the reactivity (towards reversed Boudouard gasification) of the modified char and the effect of carbonates (K_2CO_3 and Li_2CO_3) on the reactivity, thermogravimetric (TG) analysis was carried out in CO_2 atmosphere. As shown in Fig. 6, the reactivity of modified char was slightly improved compared to that of char and greatly enhanced by the addition of carbonate, especially when the temperature reached about 750℃. After only 30 minutes of reaction at 800℃, only 25.07 wt.% of the modified char-carbonate mixture remained. This result shows that the presence of carbonates can significantly catalyse the reaction between the carbon and CO_2 (Eq. 4 and Eq. 5) [5].

3.2. Electrochemical performances of different fuels

The electrochemical performances of the HDCFC using three different coal-based fuels at 750℃ are compared in Fig. 7. The OCV values are all about 0.99 V, which is close to the Nernst theoretical value, revealing the well densified electrolyte and the good sealing of the cells. It is obvious that the cell with the modified char delivered the greatest maximum power density of 366 cm^{-2} as compared to those using char (297 mW cm^{-2}) and coal (282 mW cm^{-2}). Hence, the proposed treatment of bituminous coal is effective for increasing the rate of in-situ gasification of coal.

Fig. 7(b) shows the corresponding electrochemical impedance spectra (EIS) of the HDCFCs. The intercept at high frequency is assigned to the ohmic resistance (R_o), and the arc between the two intercepts on the real axis represents the polarisation resistance (R_P). The values of R_o and R_P for the three fuels are shown in the inserted bar chart of Fig. 7(b). R_o is almost identical for all three cases, which reflects the uniform electrolyte thickness. Meanwhile, the variance of R_P is mainly due to the anode polarisation when using different fuels, decreasing in the order of bituminous coal (1.01 Ω cm^2) > char (1.00 Ω cm^2) > modified char (0.82 Ω cm^2). Therefore, the carbon oxidation activity of modified char is higher than that of other fuels. The results of electrochemical impedance spectra are thus in good accordance with the comparison of maximum power densities.

3.3. Electrochemical performances of the modified cell

To further improve the anode performance, a modified cell with Ag-infiltrated anode was tested. Fig. 8(a) shows SEM image of reduced Ag-infiltrated anode, many nanoparticles with an average size of ~40 nm were observed on the reduced anode surface. To support the nanoparticles from Ag

infiltration and examined the morphological shape of the resulting metallic silver, the lamellae was extracted from reduced Ag-infiltrated anode by FIB and then detected by TEM, and STEM combined with EDX spectroscopy. From the TEM image shown in Fig. 8(b), a plenty of blanks are observed in the lamellae, indicating the anode prepared by the tape-casting process was a porous structure with a porosity of ~40%, which benefits the diffusion of gas in anode. As shown in Fig. 8(c), some nanoparticles with diameters of approximately 35–60 nm were found on the surface of main grains. The elemental mapping shows the reduced anode are composed of Ni, Y, Zr, and Ag, and Ag shows a very uniform distribution.

Fig. 9(a) shows the electrochemical performance of the Ag-infiltrated cells fuelled using modified coal at different temperatures (750℃, 700℃, and 650℃). The maximum power density was 403 mW cm^{-2} at 750℃. Considering that this HDCFC was fuelled with modified coal, such a power density is highly attractive. With decreasing temperature, both the maximum power density and OCV value of the cell decreased dramatically, as expected theoretically.

The impact of anode infiltration with Ag on the polarisation impedance can be divided into two parts: concentration polarisation caused by mass transport resistance through the anode pores, and activation polarisation caused by charge transfer impedance at the electrochemical reaction sites [28]. It has been demonstrated that having smaller pores in the anode will reduce both the Knudsen gas diffusivity and the molecular gas diffusivity, which will increase the mass transfer resistance of the anode [29,30]. Therefore, impregnating the anode with silver nanoparticles would theoretically increase the polarisation impedance, since the silver nanoparticles occupy a small number of anode pores. In SOFCs, the Butler-Volmer equation is often used to model the activation polarisation, but this approach does not combine the microstructure and electrochemistry of the cell [31,32]. It is well known that the electrode reaction usually occurs at the region of TPB (where the electrolyte, the electrode, and the fuel meet), as experimental observation showed that an increase in the TPB length reduces activation polarisation in the anode [33]. In addition to the TPB length, the activation polarisation of an electrode for fuel oxidation is also closely related to its intrinsic activity. It was reported that Ag has much better catalytic performance than Ni additive in DCFC, possibly due to the formation of Ni_3C that inactivates the nickel [34]. Especially, recent research has shown the outstanding performance of Ag for carbon electro-oxidation [9]. Clearly, infiltrating the anode with Ag nanoparticles is expected to reduce the activation polarisation, which is much

more dominating compared to other overpotentials [28]. Therefore, the influence of Ag nanoparticle infiltration on the anode polarisation resistance should be considered in combination with the actual operating temperature. The electrochemical impedance spectra of the infiltrated cells fuelled by modified coal are shown in Fig. 9(b). The value of polarisation impedance is only 0.7 Ω cm^2 at 750°C, indicating that infiltrating the anode with Ag nanoparticles can reduce the polarisation impedance, in accordance with the electrochemical test results. Fig. 11 shows the comparison of maximum power densities of coal-based fuels applied in DCFCs. The extremely improvement are mainly contributed by the pretreatment improved the char purity and carbon electrochemical oxidation as well as infiltrating the Ni/YSZ anode with Ag nanoparticles enhanced the anode activity.

Fig. 11 shows the discharging curve of Ag-infiltrated HDCFCs that were operated with 0.4 g modified coal char as fuel and under a constant current density of 100 mA cm^{-2} at 750°C. The cell voltage decreased in the first 40 minutes and then maintained a stable value of 0.8 V for about 14.05 hours, before finally dropping rapidly and the cell stopped working. The decrease in voltage is due to the gradual loss of activated carbon particles on the surface, a decreased gasification rate, and an increase in concentration polarisation.

The Faradic efficiency (η) of carbon is an important indicator for the usability of carbon in the HDCFCs [43]. It is defined as:

$$\eta = \frac{\eta_{C^{electricity}}}{\eta_{C^{total}}} \times 100\% = \frac{\frac{It}{zF}}{\frac{m}{M}} \times 100\% = \frac{ItM}{zFm} \times 100\% \quad (10)$$

Where I and t denote the operation current and discharge time, respectively; M and m represent the molecular weight and mass of carbon; F is the Faraday constant; and z is the electron transfer number for the electrochemical oxidation of C to CO_2. The calculated Faradic efficiency of the cell after discharge (Fig. 11) is 61.06%, considering that a substantial amount of CO was generated by the reversed Boudouard reaction (Eq. 6) and exhausted from the cell. There is the potential to further increase the Faradic efficiency by optimising mass transport in the cell in up-scaled HDCFCs, e.g. CO recycling from the tail gas and expanded cell dimension. The carbon consumption was evaluated by the mass before and after the tests, which are 0.36 g and 0.01 g

respectively. The calculated fuel conversion of modified char was 97.22%, meaning that almost all the carbon in the fuel was consumed. These results mentioned above confirm the excellent electrochemical properties and stability of the Ag-infiltrated cells, strongly indicating that infiltration with Ag nanoparticles can be used to fabricate high-performance anodes for HDCFCs for either z = 4 (the main anode reaction in the HDCFC) or z = 2, corresponding to the complete or incomplete electrochemical oxidation of carbon (Eq. 4 and Eq. 5), respectively.

After the durability test, the residual of modified char-carbonate mixture was collected for further analysis. Fig. 12(a) and Fig. 12(b) show the morphology of the mixture before and after the test, respectively. While many large carbon particles were observed before the test, after the test only a few carbon particles could be found in the residual and the image was filled with mineral particles. The XRD patterns of modified char-carbonate mixture before and after the durability test are shown in Fig. 12(c) and Fig. 12(d), respectively. After the test, the two characteristic peaks of carbon became less obvious due to the consumption of carbon, which is consistent with the SEM observations. Besides potassium carbonate and lithium carbonate, lithium aluminium silicate (Li_3AlSiO_5) and potassium oxide (K_2O) were also detected in the residual of modified char-carbonate mixture. It can be inferred that Li_3AlSiO_5 was derived from the reaction between Li_2CO_3 with SiO_2 and Al_2O_3 and it could deactivate the catalyst [44]. In comparison, the reaction between K_2CO_3 with SiO_2 and Al_2O_3 occurred to a lesser degree, since no obvious peaks of the corresponding compounds were observed. Meanwhile, the peaks of K_2O were clearly observed, and they should come from the decomposition of K_2CO_3

4. Conclusion

In summary, a high-performance HDCFC was developed using nano Ag-infiltrated Ni/YSZ anode support, YSZ electrolyte, $SrSc_{0.175}Nb_{0.025}Co_{0.8}O_{3-\delta}$ cathode and modified bituminous char as fuel. It exhibited a maximum power density of 403 mW cm^{-2} at 750°C, the highest reported using coal-based fuels so far to the best of the authors' knowledge. Moreover, a high fuel conversion of 97.22% and Faradic efficiency of 61.06% were achieved, when using 0.4 g modified bituminous char as the fuel after 14.81 hours of discharge at 100 mA cm^{-2}. The excellent performance and high fuel conversion of the cell with modified bituminous char are attributed to the effective coal pretreatment method and the nano Ag-infiltrated Ni/YSZ anode with high catalytic activity. This work successfully demonstrated the feasibility of HDCFCs as a clean and efficient technology for

coal utilisation. It should be noted that higher Faraday efficiencies are expected when the cell exhaust treatment such as CO recycling from the tail gas is taken into account.

Acknowledgement

This work was supported by National Natural Science Foundation of China Project (Grant No. 51827901) and Natural Science Foundation of SZU (Grant No. 2019087). We also thank the Institute of New Energy and Low-Carbon Technology of Sichuan University and Ceshigo Research for help in characterisations.

References

[1] Zecevic S, Patton EM, Parhami P. Carbon–air fuel cell without a reforming process. Carbon 2004;42:1983–93.

[2] Liu J, Zhou M, Zhang Y, Liu P, Liu Z, Xie Y, et al. Electrochemical oxidation of carbon at high temperature: principles and applications. Energy Fuels 2018;32:4107–17.

[3] Jiang C, Ma J, Corre G, Jain SL, Irvine JTS. Challenges in developing direct carbon fuel cells. Chem Soc Rev 2017;46:2889–912.

[4] Rady AC, Giddey S, Kulkarni A, Badwal SPS, Bhattacharya S. Catalytic gasification of carbon in a direct carbon fuel cell. Fuel 2016;180:270–7.

[5] Fuente-Cuesta A, Jiang C, Arenillas A, Irvine JTS. Role of coal characteristics in the electrochemical behaviour of hybrid direct carbon fuel cells. Energy Environ Sci 2016;9:2868–80.

[6] Cao T, Huang K, Shi Y, Cai N. Recent advances in high-temperature carbon-air fuel cells. Energy Environ Sci 2017;10:460–90.

[7] Gür TM. Critical review of carbon conversion in “carbon fuel cells”. Chem Rev 2013;113(8):6179–206.

[8] Cantero-Tubilla B, Xu C, Zondlo JW, Sabolsky K, Sabolsky EM. Hybrid direct carbon fuel cell: Catalytic effect of carbonate cation and amount of carbon fuel in cell performance. Abstract 1104 in: The 221st ECS meeting; 2012.

[9] Wu H, Xiao J, Zeng X, Li X, Yang J, Zou Y, et al. A high performance direct carbon solid oxide fuel cell–A green pathway for brown coal utilization. Appl Energy 2019;248:679–87.

[10] Tang Y, Liu J. Fueling solid oxide fuel cells with activated carbon. Acta Phys-Chim Sin 2010;26:1191–4.

[11] Tang Y, Liu J, Sui J. A novel direct carbon solid oxide fuel cell. ECS Trans 2009;25:1109–14.

[12] Liu J, Yuan H, Qiao J, Feng J, Xu C, Wang Z, et al. Hierarchical hollow nanofiber networks for high-performance hybrid direct carbon fuel cells. J Mater Chem A 2017;5:17216–20.

[13] Rady AC, Giddey S, Badwal SPS, Ladewig BP, Bhattacharya S. Review of fuels for direct carbon fuel cells. Energy Fuels 2012;26:1471–88.

[14] Li X, Zhu ZH, De Marco R, Bradley J, Dicks A. Evaluation of raw coals as fuels for direct carbon fuel cells. J Power Sources 2010;195:4051–8.

[15] Miller BG. Coal energy systems. Boston, MA: Elsevier Academic Press; 2005. pp. 237–45.

[16] Yu J, Lucas JA, Wall TF. Formation of the structure of chars during devolatilization of pulverized coal and its thermoproperties: A review. Prog Energy Combust Sci 2007;33:135–70.

[17] Dudek M. On the utilization of coal samples in direct carbon solid oxide fuel cell technology. Solid State Ionics 2015;271:121–7.

[18] Fan L, Wang J, Zhao L, Hou N, Gan T, Yao X, et al. Effects of surface modification on the reactivity of activated carbon in direct carbon fuel cells. Electrochim Acta 2018;284:630–8.

[19] Gu H, Ran R, Zhou W, et al. Anode-supported ScSZ-electrolyte SOFC with whole cell materials from combined EDTA–citrate complexing synthesis process. Journal of Power Sources, 2007, 172(2): 704–712.

[20] Yang G, Su C, Wang W, et al. Single-chamber solid oxide fuel cells with nanocatalyst-modified anodes capable of in situ activation. Journal of Power Sources, 2014;264: 220–228.

[21] Jiao Y, Zhao J, An W, Zhang L, Sha Y, Yang G, et al. Structurally modified coal char as a fuel for solid oxide-based carbon fuel cells with improved performance. J Power Sources 2015;288:106–14.

[22] Hibino T, Kobayashi K, Heo P. Oxygen reduction reaction over nitrogen-doped graphene oxide cathodes in acid and alkaline fuel cells at intermediate temperatures. Electrochim Acta 2013;112:82–9.

[23] Livneh T, Bar-Ziv E, Senneca O, Salatino P. Evolution of reactivity of highly porous chars from Raman microscopy. Combust Sci Technol 2000;153(1):65–82.

[24] Song Y, Jiang B, Mathews JP, Yan G, Li F. Structural transformations and hydrocarbon generation of low-rank coal (vitrinite) during slow heating pyrolysis. Fuel Process Technol 2017;167:535–44.

[25] Manoj B, Kunjomana AG. Chemical leaching of an Indian bituminous coal and characterization of the products by vibrational spectroscopic techniques. Int J Miner Metall Mater 2012;19(4):279–83.

[26] Sharma RK, Wooten JB, Baliga VL, Lin X, Chan WG, Hajaligol MR. Characterization of chars from pyrolysis of lignin. Fuel 2004;83:1469–82.

[27] Eom S, Ahn S, Kang K, Choi G. Correlations between electrochemical resistances and surface properties of acid-treated fuel in coal fuel cells. Energy 2017;140:885–92.

[28] Lu Y, Gasper P, Pal U B, et al. Improving intermediate temperature performance of Ni-YSZ cermet anodes for solid oxide fuel cells by liquid infiltration of nickel nanoparticles. Journal of Power Sources, 2018, 396: 257–264.

[29] Kong W, Zhu H, Fei Z, Lin Z. A modified dusty gas model in the form of a Fick's model for the prediction of multicomponent mass transport in a solid oxide fuel cell anode. J Power Sources 2012;206:171–8.

[30] Leonide A, Apel Y, Ivers-Tiffée E. SOFC modeling and parameter identification by means of impedance spectroscopy. ECS Trans 2009;19(20):81–109.

[31] Sonn V, Leonide A, Ivers-Tiffée E. Combined deconvolution and CNLS fitting approach applied on the impedance response of technical Ni/8YSZ cermet electrodes. J Electrochem Soc 2008;155(7):B675–9.

[32] Njodzefon J-C, Klotz D, Kromp A, Weber A, Ivers-Tiffée E. Electrochemical modeling of the current-voltage characteristics of an SOFC in fuel cell and electrolyzer operation modes. J Electrochem Soc 2013;160(4):F313–23.

[33] Lee K T, Vito N J, Wachsman E D. Comprehensive quantification of Ni-$Gd_{0.1}Ce_{0.9}O_{1.95}$ anode functional layer microstructures by three-dimensional reconstruction using a FIB/SEM dual beam system. Journal of Power Sources, 2013, 228: 220-228.

[34] Dudek M, Tomczyk P. Composite fuel for direct carbon fuel cell. Catal Today 2011;176:388–92.

[35] Ahn SY, Eom S Y, Rhie YH, et al. Application of refuse fuels in a direct carbon fuel cell system[J]. Energy, 2013;51:447–456.

[36] Ju H K, Eom J, Lee J K, et al. Durable power performance of a direct ash-free coal fuel cell. Electrochimica Acta, 2014, 115: 511–517.

[37] Jiang C, Ma J, Arenillas A, et al. Hybrid direct carbon fuel cells with different types of mineral coal[J]. ECS Transactions, 2013;57(1):3013–3021.

[38] Dudek M, Tomczyk P, Socha R, et al. Use of ash-free “Hyper-coal” as a fuel for a direct carbon fuel cell with solid oxide electrolyte. International journal of hydrogen energy, 2014;39(23):12386–12394.

[39] Jiao Y, Xue X, An W, et al. Purified high-sulfur coal as a fuel for direct carbon solid oxide fuel cells. International Journal of Energy Research, 2019;43(7): 2501–2513.

[40] Dudek M. On the utilization of coal samples in direct carbon solid oxide fuel cell technology. Solid State Ionics, 2015;271: 121–127.

[41] Rady AC, Giddey S, Kulkarni A, et al. Direct carbon fuel cell operation on brown coal. Applied energy, 2014;120: 56–64.

[42] Jewulski J, Skrzypkiewicz M, Struzik M, et al. Lignite as a fuel for direct carbon fuel cell system. international journal of hydrogen energy, 2014;39(36): 21778–21785.

[43] Xiao J, Han D, Yu F, Zhang L, Liu J, Zhan Z, et al. Characterization of symmetrical $SrFe_{0.75}Mo_{0.25}O_{3-\delta}$ electrodes in direct carbon solid oxide fuel cells. J Alloys Compd 2016;688:939–45.

[44] Tang J, Wang J. Catalytic steam gasification of coal char with alkali carbonates: A study on their synergic effects with calcium hydroxide. Fuel Proc Technol 2016;142:34–41.

List of Figures

List of Tables

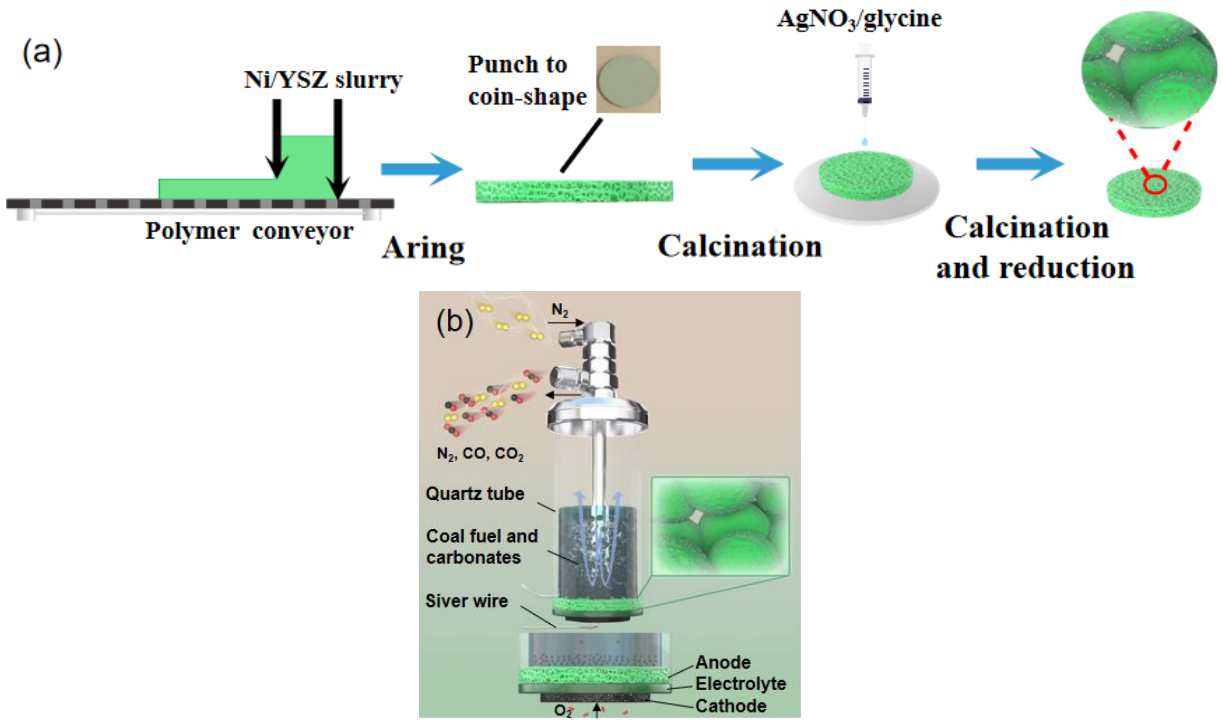

Figure 1 (a) Process of Ag nanoparticles infiltration, (b) Schematic of the coal-fuelled single HDCFC.

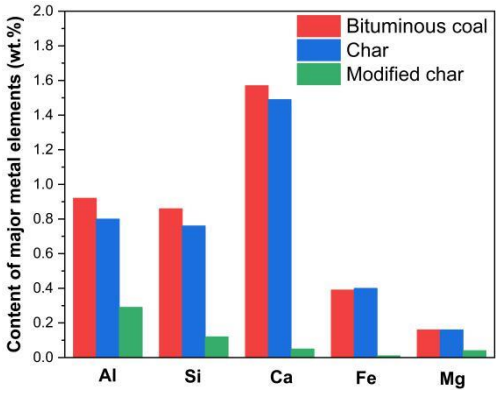

Figure 2 Metal element contents of bituminous coal, char, and modified char.

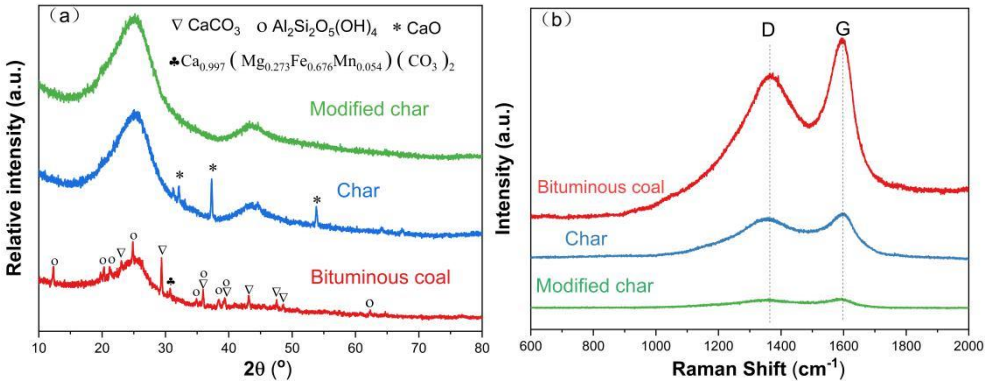

Figure 3 (a) XRD patterns and (b) Raman spectra of bituminous coal, char and modified char.

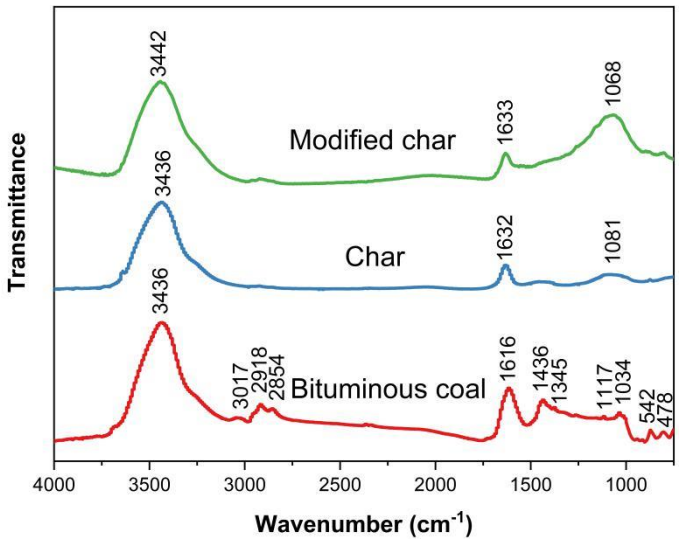

Figure 4 Fourier transform infrared spectra of bituminous coal, charm and modified char.

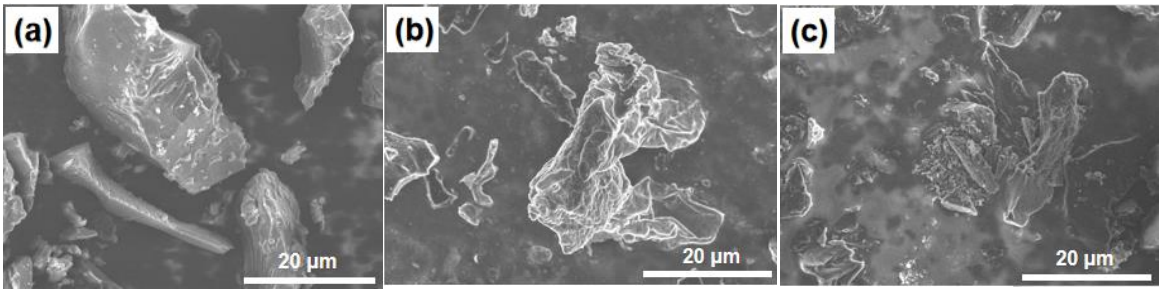

Figure 5 SEM images of (a) bituminous coal, (b) char and (c) modified char.

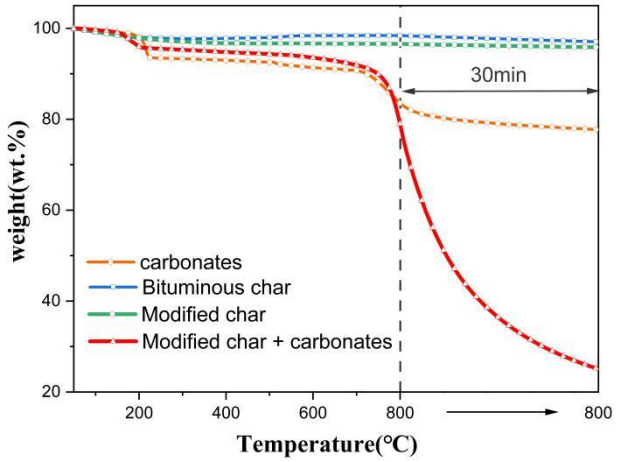

Figure 6 Thermogravimetric curves of char and modified char-carbonate mixture under CO_2 atmosphere.

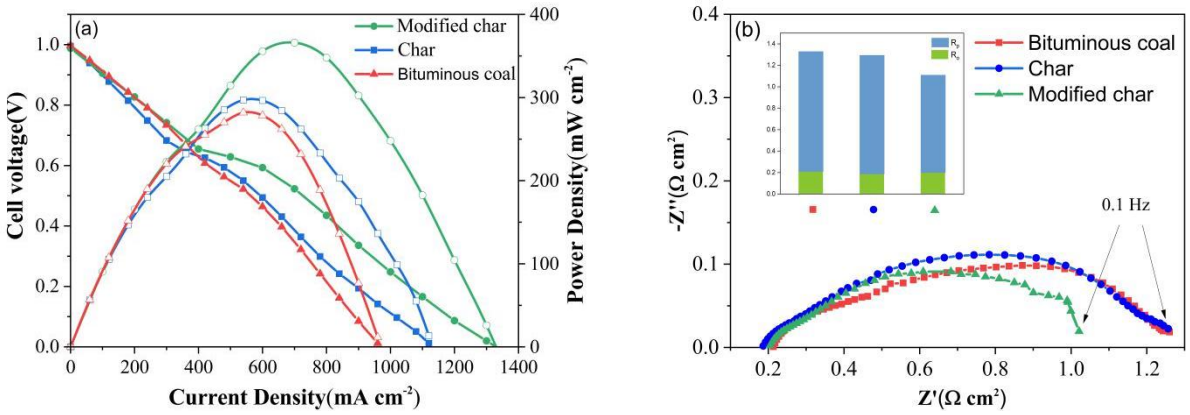

Figure 7 Performance of HDCFCs with bituminous coal, char, and modified char: (a) I-V and I-P curves, (b) EIS under OCV with the corresponding ohmic resistance (R_o) and polarisation resistance (R_P) (inset).

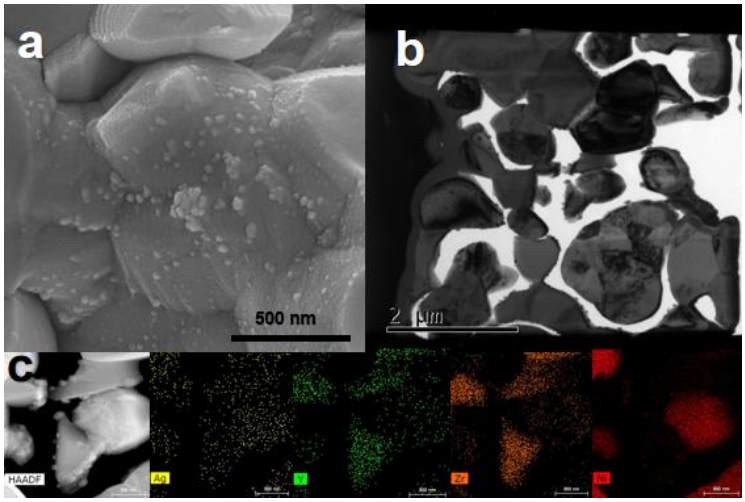

Figure 8 (a) SEM images of reduced Ag-infiltrated anode, (b) TEM images of the lamellae extracted from reduced Ag-infiltrated anode, (c) STEM-EDX results of reduced Ag-infiltrated anode

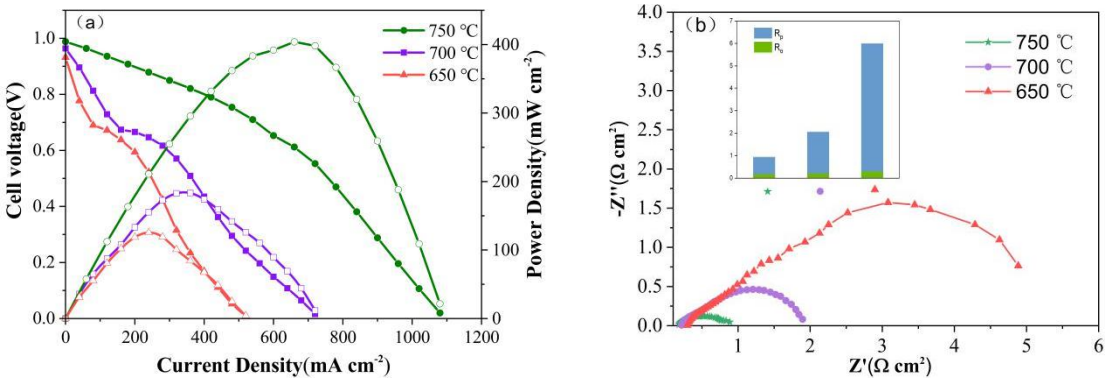

Figure 9 Performance of Ag-infiltrated HDCFCs fuelled by modified char: (a) I-V and I-P curves, (b) EIS under OCV with the corresponding ohmic resistance (R_o) and polarisation resistance (R_P) (inset).

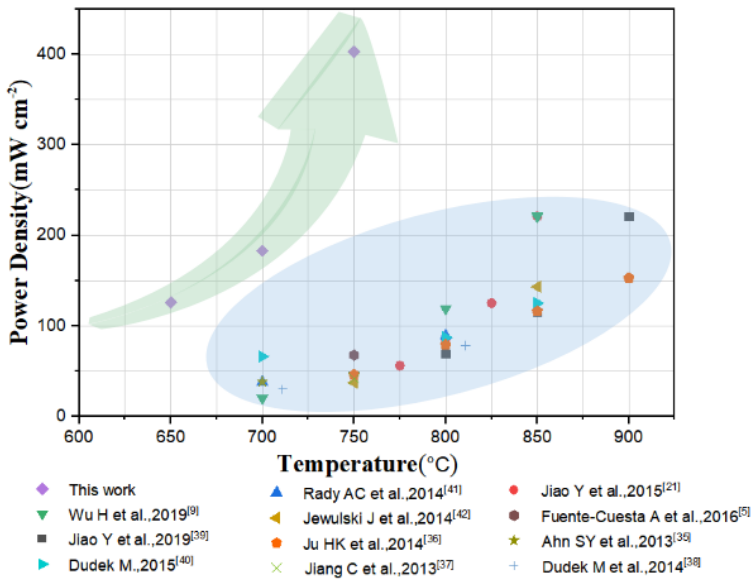

Figure 10 Comparison of maximum power densities of coal-based fuels applied in DCFCs.

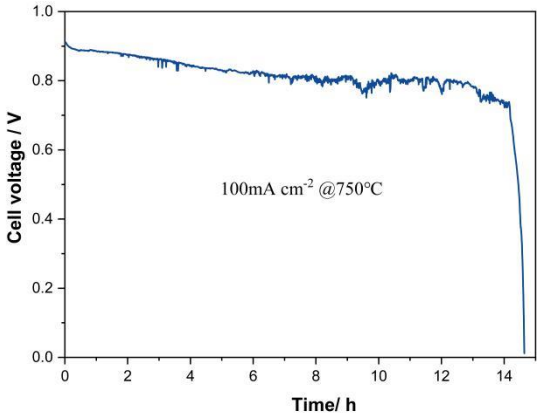

Figure 11 Discharge curve of HDCFC operated with Ag-infiltrated cells and fuelled by modified coal.

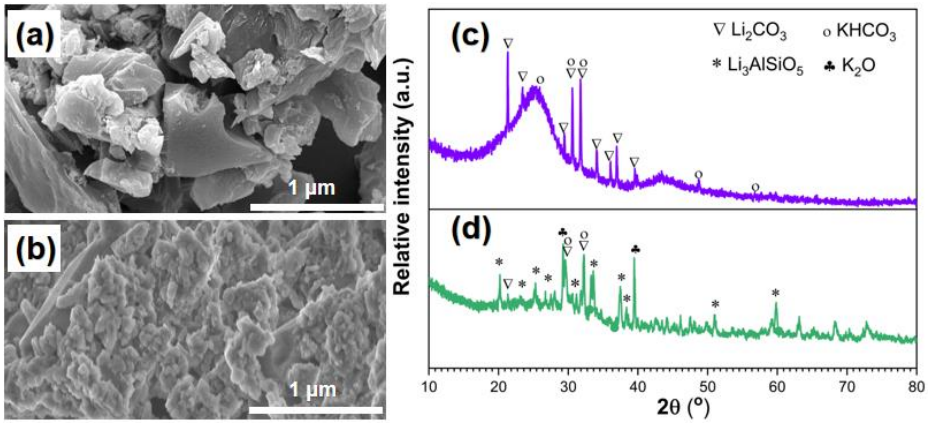

Figure 12 (a–b) SEM images and (c–d) XRD patterns of the modified char-carbonate mixture before and after stability test.

List of Tables

Table 1 Organic element contents of bituminous coal, char and modified char.

Samples	Wt.% C	Wt.% H	Wt.% O	Wt.% N	Wt.% S
Bituminous coal	80.99	4.18	5.47	1.52	0.44
Char	84.71	1.61	2.87	1.45	0.39
Modified char	89.18	2.78	0.61	1.53	0.38

Table 2 Integrated peak area of the three main functional groups ($A_{C=O}$, A_{O-H}, A_{C-O}) and their ratios.

Samples	Integral peak area			Ratio		
	$A_{C=O}$	A_{O-H}	A_{C-O}	$A_{O-H}/A_{C=O}$	$A_{C-O}/A_{C=O}$	$(A_{O-H}+A_{C-O})/A_{C=O}$
Bituminous coal	5.21	36.01	6.22	6.91	1.19	8.10
Char	2.76	33.50	5.73	12.14	2.08	14.22
Modified char	3.29	41.63	28.88	12.28	8.52	20.76

Table 3 Textural properties of bituminous coal, char, and modified char.

Samples	N_2 adsorption		
	S_{BET} (m^2g^{-1})	D_{pore} (nm)	V_{micro} (cm^3g^{-1})
Bituminous coal	2.0455	5.5445	0.003844
Char	7.1734	13.8713	0.008355
Modified char	4.254	6.5945	0.003052